JACS
JOURNAL OF THE AMERICAN CHEMICAL SOCIETY

ARTICLE

pubs.acs.org/JACS

(Barely) Solid $Li(NH_3)_4$: The Electronics of an Expanded Metal

Eva Zurek,[†] Xiao-Dong Wen,[‡] and Roald Hoffmann[‡]

[†]Department of Chemistry, State University of New York at Buffalo, 331 Natural Sciences Complex, Buffalo, New York 14260, United States

[‡]Department of Chemistry and Chemical Biology, Cornell University, Baker Laboratory, Ithaca, New York 14853, United States

Supporting Information

ABSTRACT: The highly expanded metal, lithium(0)tetraamine, and its electronic structure is as full of complexity and surprises as the lithium solutions in anhydrous ammonia from which it crystallizes at 90 K. Our theoretical studies of the Phase II, $Z = 8$, $I\bar{4}3d$ structure of this material reveal that the molecular building block is an almost ideal tetrahedron, in agreement with recent experiments. Close in enthalpy at $P = 1$ atm, and consistent with the low melting point, are bcc and Cs−IV configurations. Under pressure, the $I\bar{4}3d$ structure emerges as more stable than its alternatives. In this phase six relatively narrow bands, four of them occupied, separate from the conduction and valence bands. We trace these bands to pockets of electron density arising between sterically encumbered ammonias, six such pockets in the $Z = 8$ unit cell. The observed band structure can be explained by considering a Jortner−type model, where pseudoatoms are placed in these holes. The electride $Li(NH_3)_4$, while not a very good metal, is a unique material, by virtue of its low melting point.

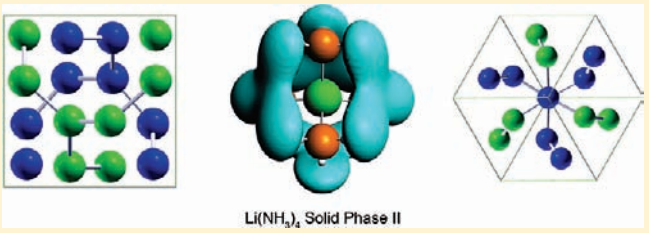

1. INTRODUCTION

Given what one knows of the remarkable alkali−metal ammonia solutions[1]—a molecular liquid dissolving much metal, with striking volume expansion, a lively blue or magnificent gold color, unusual magnetism, a conductivity rising with concentration from ionic to greater than that of mercury, a liquid−liquid phase separation—one should not be astonished that the lithium−ammonia system harbors still another surprise.

More than 120 years ago Joannis carried out the first crystallization of alkali metals (Na and K) dissolved in ammonia.[2] In 1898 Moissan extended this work to Li and Ca.[3] He was the first to report the existence of the bronze solid "lithium ammonium" ($LiNH_3^-$)—now known to be $Li(NH_3)_4$. Seventy years later Mammano and Sienko revisited this system and found that cooling a saturated (20 mol percent metal, MPM) solution yielded a stable crystalline solid.[4] But only at 89 K, making $Li(NH_3)_4$ *the lowest melting point metal known*. Solid $Li(NH_3)_4$ can be viewed as an expanded metal compound—one in which the distance between the molecular bearers of the eventually itinerant electrons becomes large. And we do mean large: in the $P = 1$ atm structure of $Li(NH_3)_4$ at 40 K the smallest center to center separation of the radicals is 5.25 Å. Other expanded metals include $A(NH_3)_6$ where A = Ca, Sr, Ba, Eu, or Yb.[5]

It has not been easy to determine the structures of the different phases of lithium(0) tetraamine. A re−evaluation[6] of powder X−ray[4] and neutron diffraction[7] data led to the conclusion that $Li(NH_3)_4$ has three stable phases, with body−centered−cubic structures based upon the packing of the quasi−spherical $Li(NH_3)_4$ molecular complexes. Phase I, stable between 82 and 89 K, was thought to be an orientationally disordered plastic phase, whereas phase II (25−82 K) appeared to crystallize in space group $I\bar{4}3d$. Below 25 K extra reflections in the neutron diffraction data indicated the formation of phase III, a superstructure with possible antiferromagnetic ordering. Strong isotope effects are present, since only phase II and III have been observed for $Li(ND_3)_4$.

Further experimental work[8] on $Li(ND_3)_4$ confirmed the $I\bar{4}3d$ space group assignment of ref 6 for phase II. In this study, the molecular complex was now found to be strongly distorted, with one Li−N bond (2.488 Å) significantly longer than the other three (1.984 Å). Recently, the structure has been re−examined with high quality neutron powder diffraction.[9] The space group was determined to be the same, but the molecular complex was found to possess nearly equivalent Li−N bonds (2.036 and 2.078 Å at 40 K; similar data was obtained at 75 K). The ND_3 groups were pyramidal, as expected, with an average H−N−H angle of 103.3°. At 10 K phase III was found to have space group $P2_13$, and the deviation from the ideal tetrahedral geometry of the molecular units was negligible.

Whereas the conductivity of a saturated metal−ammonia solution is high, the unusual magnetic,[10−12] and electrical[13]

Received: October 28, 2010
Published: February 22, 2011

   dx.doi.org/10.1021/ja109397k | J. Am. Chem. Soc. 2011, 133, 3535–3547

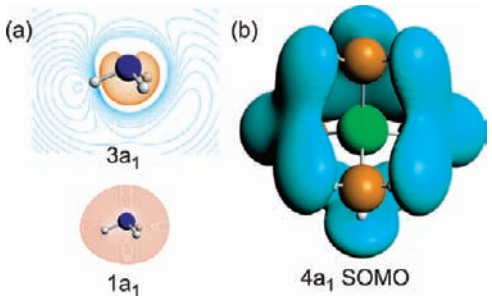

Figure 1. (a) Contour diagrams of the $1a_1$ and $3a_1$ ammonia orbitals calculated using atom−centered basis sets.[1] (b) An isosurface (±0.02 au) of the $4a_1$ SOMO of $Li(NH_3)_4$.[1] Nitrogens are colored as blue, hydrogens as white, and lithium as green.

properties of solid $Li(NH_3)_4$ hint that it may be just on the metallic side of a metal−to−insulator transition. The Hall coefficient indicates that the liquid and solid phase I are nearly free electron metals, whereas solid phase II has fewer carriers.[13] Magnetically, solid phase I appears to be an ordered version of the liquid, and both exhibit nearly−free−electron like behavior.[11,12] The susceptibility measurements indicate that below 25 K the spin polarons become antiferromagnetically ordered.[11,12] Sienko et al. attributed the large change in the susceptibility of solid phase II to an electronic effect and the decreased metallicity (increased resistivity) to a small structural distortion within the cubic system. They also proposed that a further lattice distortion in solid phase III opens up a pseudo−gap in the density of states of the material; phase III is even less metallic than phase II.

Various computational studies have considered the $Li(NH_3)_4$ molecule[14−16] and $[Li(NH_3)_4]_n$ clusters.[1] Kohanoff et al. performed plane−wave DFT calculations on an isolated molecule as well as a model for solid phase II.[17] For the latter, they employed a primitive cell containing 8 formula units in space group $I\bar{4}3d$ and a lattice parameter of 14.83 Å. The positions of the atoms in the molecular entities were optimized, but the cell was kept fixed. The delocalized spatially extended singly occupied molecular orbital (SOMO) of the molecule made up the conduction band of the solid. The electron density associated with the conduction band only partially filled the cavities and seemed to "wet" the hydrogens.

In a recent study we looked in excruciating detail at the molecular species present in lithium−ammonia solutions of varying concentration.[1] Here this work is extended to the solid.

2. THE $Li(NH_3)_4$ MONOMER

To begin to understand the electronic structure of solid $Li(NH_3)_4$, we need detailed knowledge of the isolated $Li(NH_3)_4$ monomer—the unit from which the solid is constructed. In our previous molecular calculations using atom−centered basis sets[1] we showed that the occupied Li 2*s* as well as unoccupied Li (3*s*, 4*s*) functions contribute to the singly occupied molecular orbital, SOMO, of $Li(NH_3)_4$ (Figure 1(b)). Other orbitals mix in as well. The nearly spherical region around N arises from the admixture of the formally occupied ammonia $1a_1$ orbitals. Importantly, the SOMO also contains contributions from the unoccupied $3a_1$ σ^* NH_3 orbitals, which are very diffuse and have a node near H. These important $1a_1$ and $3a_1$ ammonia MOs are illustrated in Figure 1(a).

As a result of the $3a_1$ admixture, the SOMO has the lovely quadruple clover−leaf pattern of Figure 1(b). The probability to find the excess electron in the SOMO a distance *r* away from the Li atom ($P(r)$) has a maximum 1.2 Å further out than the hydrogens and decreases slowly, falling to $P(r) = 0.01\%$ approximately 9 Å away from the Li atom. An important consequence of the a_1 symmetry of the SOMO is a bonding interaction between hydrogen atoms from neighboring ammonias. In our molecular study, we introduced a symbol, H←〰→H, to signify the weak but numerous orbital−mediated bonding interactions between any two hydrogens in this SOMO.

Table 1. Energy (in eV per $Li(NH_3)_4$ Unit) of Various Solid $Li(NH_3)_4$ Structures Given with Respect to the Isolated Molecule (Spin−Polarized, Plane−Wave Calculation)[a,e]

system	ΔE	Li−N	H−N	*a*
Phase II_{SP}[b]	−0.042	2.035, 2.078	0.97−1.01	14.837
Phase II_{fixed}[b]	−0.640	2.115, 2.117	∼1.03	14.837
Phase II_{all}[b]	−0.659	2.120, 2.121	∼1.03	15.193
Phase III_{SP}[c]	0.899	1.87−2.16	0.86−1.10	14.783
sc[d]	−0.613	2.119	1.029	6.196
fcc[d]	−0.497	2.087	1.027	10.950
bcc[d]	−0.652	2.107	1.029	7.873
Cs−IV	−0.652	2.125	1.029	10.125
$P2_13$	−0.593	2.116	1.030	9.903

[a] "SP" denotes a single−point calculation; "fixed": one in which the ionic positions may vary, but the lattice parameters are fixed; "all": one in which all parameters are allowed to optimize. [b] 40 K phase II structure determined in ref 9. [c] 10 K phase III structure determined in ref 9. [d] sc−simple cubic; fcc−face centered cubic; bcc−body centered cubic. [e] The three structures with the lowest energy (Phase II_{all}, bcc, Cs−IV) are highlighted in bold. We also provide the Li−N and N−H distances as well as the lattice parameter (*a*) in Å.

3. STRUCTURAL ALTERNATIVES FOR SOLID $Li(NH_3)_4$ AT 1 ATM

$Li(NH_3)_4$ has a very low melting point, suggesting that arrangements other than the one observed might have similar enthalpies. For this reason we looked not only at the observed structure but also at an assortment of hypothetical geometries. It should be noted that our calculations are at 0 K; experiment has shown that the structural parameters of the crystalline $Li(NH_3)_4$ depend on the temperature and that there is a significant isotope effect.

For the phase II structure determined at 40 K in ref 9 we have (i) performed a single−point calculation (denoted "*SP*" in Table 1); (ii) optimized the atomic positions of this structure, keeping the lattice constants fixed ("*fixed*"); and (iii) carried out a full structural relaxation ("*all*"). Calculations (i) and (ii) were also performed using the phase II structural parameters determined in ref 8—those of the strongly distorted $Li(ND_3)_4$ complex. This system was of substantially higher energy and optimized to give a more symmetrical $Li(NH_3)_4$ structure (see the Supporting Information, SI). Moreover, a single−point calculation on the 10 K phase III system (neglecting magnetism) was performed. We did not optimize the latter, since it has 16 formula units in the primitive cell, and the possibility of antiferromagnetic order would make this a daunting calculation.

Could more symmetrical geometries compete? Simple cubic (sc), body centered cubic (bcc), and face centered cubic (fcc) arrangements of the $Li(NH_3)_4$ units were also studied. In addition, we looked at a "Cs−IV" geometry, in which the $Li(NH_3)_4$ units were placed at the positions of the Cs atoms in this high pressure phase of cesium.[18] The resulting structure had

the same space group as the parent from which it was derived, $I4_1/amd$. This space group was chosen since it is a common theme for many compressed alkali metals—Rb−V crystallizes in it,[19] and theoretical work indicates that certain phases of compressed K[20] and H[21] may as well. A recent computational study predicted that elemental Li would have the $P4_132$ structure above 300 GPa.[20] Thinking from the "expanded metal" perspective, we have replaced the lithiums by $Li(NH_3)_4$ units in this system; the resulting structure had a somewhat different space group (since the molecular units are not completely spherical), $P2_13$. Even though they have the same space group, this structure differs from the one determined for phase III in ref 9.

A single−point calculation on the 40 K crystal structure from ref 9 showed that it is only 0.042 eV per monomer lower in energy than the isolated (fully optimized) $Li(NH_3)_4$ molecule. When the atomic positions were relaxed, but the lattice constants were fixed, the energy decreased substantially, by 0.598 eV. During the optimization the relative position of the $Li(NH_3)_4$ units (x positional parameter) barely changed, so the lower energy of the optimized structure was primarily due to geometry changes *within* the molecular units. Experimentally, the N−D bonds were found to be between 0.972 and 1.013 Å, whereas the calculated N−H ones are 1.030/1.031 Å. The Li−N bond lengths stretched from 2.035/2.078 Å to 2.115/2.117 Å upon relaxation.

If we also optimize the lattice parameters, the energy decreases by only a further 0.019 eV per $Li(NH_3)_4$ unit. During the optimization a increases from 14.837 to 15.193 Å, whereas the relative position of the molecular units, and their internal geometries, does not change much. All of the Li−N bonds are nearly equivalent: three of them are 2.121 Å, and one is 2.120 Å. The N−Li−N angles are 109.24/109.70°, the N−H bonds are almost all the same length (1.029/1.030 Å), and the H−N−H angles fall between 105 and 106°. The structural parameters are very similar to those determined for the isolated molecule — the molecular complex in the solid is nearly tetrahedral.

These calculations indicate that the difference in energy between the fully optimized and the experimentally determined phase II structure is primarily due to geometrical changes within the molecular units (∼97%). In particular the calculated Li−N and N−H distances are longer than those experimentally determined for the deuterated compound. Bonds to deuterium are somewhat stronger (and shorter) than the corresponding bonds with hydrogen, so the density of *heavy* water is 11% greater than that of normal water itself.[22] This is likely one of the reasons for the difference between the experimentally determined structure and the one computed here.

The cubic lattice parameter decreases as the temperature is lowered.[9] For the deuterated phase II structure at 40 K, a = 14.837 Å, so at 0 K, one would expect a to be somewhat smaller still. The lattice constant we find is, on the other hand, somewhat larger, 15.193 Å. Part of the reason for this is because of the longer Li−N and Li−H distances we calculate in the extended structure. It may also be that the DFT functional we adopted is inadequate for the large dispersion forces likely to exist in this system. Should we worry about a 2.4% difference between the two sets of lattice constants? Probably not, especially taking into account the fact that one would expect the deuterated system to be somewhat more dense.

A single−point calculation on phase III showed that its energy is substantially higher than any other structure we considered. Perhaps this is because the structure of the experimentally determined deuterated system has some extraordinarily short Li−N (1.87 Å) and N−D (0.86 Å) bonds. Presumably, an optimization (which we could not afford) would yield a more stable structure in which all of the Li−N and N−H bonds elongate. Another potential source of error is that we did not take into account possible magnetic ordering in our calculation.

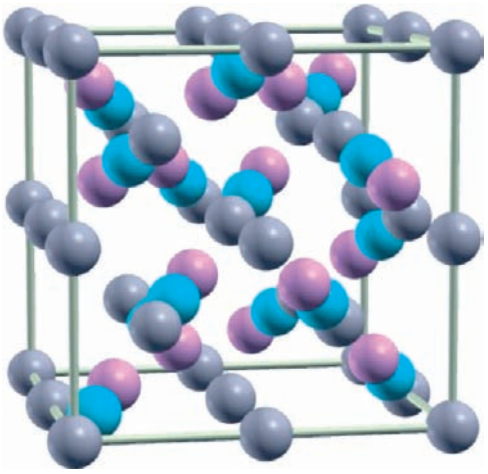

Figure 2. An illustration of how shifting the Li* pseudoatoms along the body diagonal takes a supercell of the bcc cell into the $I\bar{4}3d$ structure. The gray Li* are for a bcc structure. They move to the positions of the blue, and pink Li* when x is varied. The gray pseudoatoms on the border of the unit cell move outside of the cell during the shift (not shown).

From a comparison of the structural models we considered (Table 1, ΔE per $Li(NH_3)_4$ unit for all structures), we find the relaxed phase II structure to be the most stable (ΔE=−0.659 eV). But not by much; the bcc and Cs−IV geometries have almost the same energy per formula unit (ΔE=−0.652 eV). The closeness of the enthalpy of several quite distinct structures is a hallmark of a system approaching the liquid state.[23] And since solid $Li(NH_3)_4$ is the lowest melting point metal known, one would expect many structures to be nearly isoenergetic, at least at normal pressures.

In our molecular calculations, dimers and trimers of $Li(NH_3)_4$ with S = 0 were found to be more stable than the monomer by ∼0.17 eV per $Li(NH_3)_4$. In comparison, solid phase II, in which each molecule makes more contacts with its neighbors, is about 4 times more stable.

Given how close the energies of the three $Li(NH_3)_4$ structures highlighted in bold in Table 1 are, we have to face the question of "Is there a barrier between bcc, Cs−IV and the relaxed phase II?" Let us think about their basic geometries, ignoring internal rotations of $Li(NH_3)_4$. One could ask this question in another way: if we replace the molecular $Li(NH_3)_4$ unit by a pseudoatom, call it Li*, what motions of Li* take one structure into the other. The $I\bar{4}3d$ structure can easily be derived from a 2 × 2 × 2 supercell of the bcc lattice (space group $Im\bar{3}m$).[24] One can consider the supercell as being composed of equidistant Li* pseudoatoms running parallel to the body diagonals (four equivalent ⟨111⟩ directions). Shifting the atoms along the body diagonals gives the $I\bar{4}3d$ structure, as illustrated in Figure 2. Interestingly, in the pressure range of ∼40−70 GPa, elemental Li also crystallizes in this space group.[24] The positional parameter x defines how much the atoms are shifted; for a bcc cell x = 0, for elemental Li x = 0.045−0.060 and for the experimentally determined phase II structure, x∼0.1. When x = 0.25, we once again get a bcc cell.

dx.doi.org/10.1021/ja109397k |*J. Am. Chem. Soc.* 2011, 133, 3535–3547

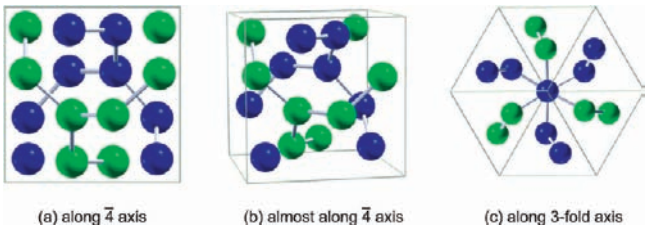

Figure 3. Three views of the conventional unit cell of the $I\bar{4}3d$ structure. The blue and green Li* pseudoatoms represent the center of the $Li(NH_3)_4$ monomers, which form two interpenetrating nets. The lines do not represent bonds but are given to guide the eye.

One may envisage the bcc structure as a stacking of square nets in the *xy* plane. The first net, **A**, contains an atom at the origin of the coordinate system. The second net, "up" in the *z* direction, call it net **B**, is centered by an atom at (1/2,1/2,1/2). The next layer will be **A** and so on, such that the layering in the bcc structure is given by **ABABA**... . The Cs−IV structure is also built up from square nets, but, in addition to **A** and **B**, there are also **C** and **D** nets centered at $(0, 1/2, z_c)$, and $(1/2, 0, z_d)$, respectively. The layering in the Cs−IV structure is given by **ACBDA**... . One way this structure may be transformed to a bcc cell is by shifting the **C**, **B**, and **D** layers in their *xy* planes so that they have the same centering as **B**, **A**, and **B**, respectively.

The $I\bar{4}3d$ structure of $Li(NH_3)_4$ is so special (and beautiful) that it is worthwhile to become better acquainted with it. The internal details of the $Li(NH_3)_4$ monomer units comprising the structure obscure the underlying connectivity. So let us get an overview by regarding each monomer as a pseudoatom. Figure 3 gives three views of the lattice, two along the $\bar{4}$ and a 3−fold axis, and a third one slightly offset from the $\bar{4}$, so as to emphasize the connections within the networks. One can see the lovely interpenetrating trivalent nets, with distances between adjacent monomers of 5.371 Å within one net and 6.579 Å between nets. The nets are indeed tightly coupled.

4. ELECTRONIC STRUCTURE OF SOLID $Li(NH_3)_4$ AT 1 ATM

In Figure 4 we compare the densities of states (DOS) near the Fermi level of the optimized phase II and bcc structures. Note the small energy window here, which covers essentially only the valence states arising from the $4a_1$ monomer SOMO, or the "metal−forming" bands. While the energies of the two structures are nearly the same, their electronic structures are quite distinct. Interestingly, the phase II structure has a pseudogap at the Fermi level (as does pure compressed Li with the same space group[24]), whereas the bcc alternative does not have a pseudogap. In ref 17 the Fermi level was calculated to lie on a peak in the DOS. The finding that the structural distortion from bcc to $I\bar{4}3d$ causes $Li(NH_3)_4$ to become less metallic is in agreement with experiments that show phase II to have decreased metallicity as compared with the liquid as well as the orientationally disordered solid phase I.[11−13]

Actually, two other structures we studied had pseudogaps at the Fermi level. As Figure 4 shows both the Cs−IV and phase III structures had a somewhat lower $g(E_F)$/valence electron than phase II. Should we trust the DOS for phase III, since its structure was not optimized? In our study we found that the valence DOS for all of the phase II systems we considered (*SP*, *fixed*, or *all* in Table 1) was very similar, see the SI. On the other hand, the position and bandwidth of other lower energy states did depend upon the geometry of the molecular complex. These lower bands arise from the interaction of the ammonia lone pairs with the Li $2s/2p$ orbitals, so it is not surprising that their breadth correlates with the deviation of the $Li(NH_3)_4$ unit from ideal tetrahedral symmetry. Thus, it seems plausible that the valence DOS of phase III would not change much if the structure were fully optimized (which, as we remind the reader, we were unable to do). On the other hand, we expect an optimization to affect the DOS of the other lower energy states to a larger extent, due to a change in the Li−N/N−H bond lengths. If this conjecture is correct, our results would be in−line with experimental observations that phase III is even less metallic than phase II.[11−13] Interestingly, the bcc and Cs−IV systems were isoenergetic; however, only the latter structure has a pseudogap at E_F.

The actual electron density in the states involved in metallization is of interest. One could examine the states within an energy window, $\Delta\varepsilon$, around E_F. We have chosen to look at the bands formed from the SOMO that are filled, i.e. integrating the occupied states in Figure 4 for $-1.2 \leq \varepsilon \leq 0$ eV.

First, let us consider the electron density of the bcc lattice, since it is easier to visualize than that of phase II. The maximum density is directly around the nitrogen atoms. If the value of the isosurface is decreased a little bit, another region — a small distance further out than the hydrogens — appears. Decreasing the isosurface value causes these regions to become larger, until they eventually grow together, forming winding channels connecting the hydrogens, as illustrated in Figure 5(a). These regions of continuous electron density describe the place where H⟵⟶H bonding interactions occur. For comparison, the density obtained from our plane−wave calculations for the SOMO of the monomer is shown in Figure 5(c). The maximum density is also found around the nitrogen atoms, and the cloverleaf lobes (described above) are a result of H⟵⟶H bonding interactions. Clearly, in the bcc structure the density from directly below the valence band up to E_F emerges from the overlap of these $4a_1$ SOMOs of the constituent $Li(NH_3)_4$ molecules shown in Figure 5(c). Note that the charge density associated with the SOMO in the isolated molecule is similar to that obtained in previous plane−wave results.[17]

The electron density of phase II− $Li(NH_3)_4$ in Figure 5(b) (again integrated over the occupied part of the SOMO band) is similar. The largest isovalues are around the nitrogen atoms. Upon decreasing the isosurface values, other areas in the middle of nonspherical cavities toward which some of the hydrogens point begin to appear. The distance between two hydrogens facing each other in such a cavity is 4.7−5.6 Å. This is somewhat larger than in the solvated electron, $e^-@(NH_3)_n$, species or in the $Li(NH_3)_4$ clusters which we studied in our molecular computations (the distances between nearest neighbor hydrogen atoms was computed to be around 3 Å).[1]

In the plane−wave calculations, as the electron density isovalue is decreased, the yellow regions in the cavities grow toward the hydrogens which face the center of the cavity. Thus, the phase II structure also exhibits H⟵⟶H bonding. Here we find the maximum isovalues to be around the nitrogen atoms. The second highest isovalues are *near the center of the cavities*. In the bcc structure and also in the molecular systems[1] the maxima of the electron density were found to be near the nitrogen atoms and close to the hydrogen atoms. It is not quite clear to us why this difference occurs. Perhaps in the phase II structure the geometry is such that the maximum overlap of the diffuse lobes

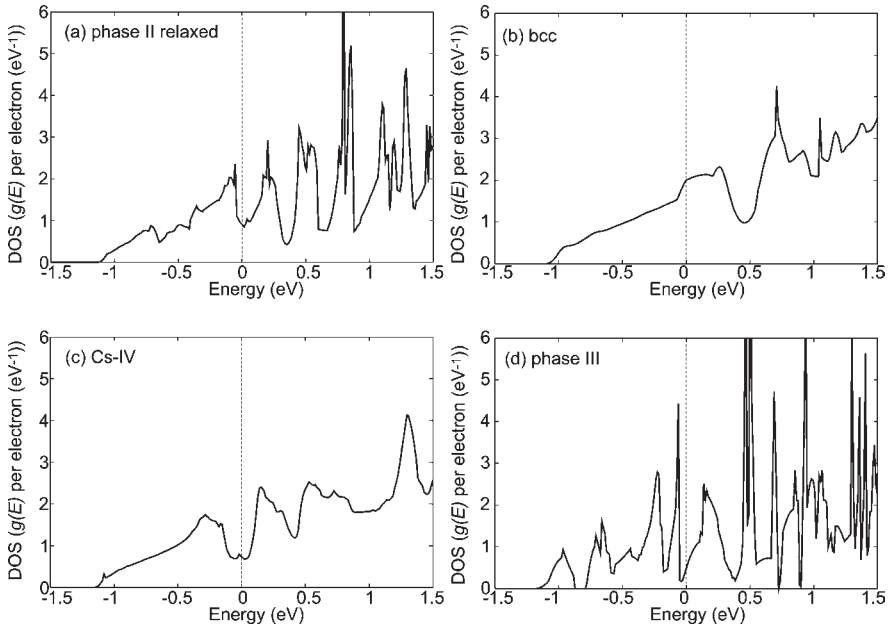

Figure 4. Valence DOS ($g(E)$/excess electron in eV^{-1}) of the fully optimized geometries of (a) phase II, (b) bcc, and (c) the Cs−IV type structures of $Li(NH_3)_4$, as well as of (d) the experimentally determined phase III. The dashed vertical lines is the Fermi energy, E_F. For the phase II, Cs−IV type, and phase III structures it falls in a pseudogap, whereas for the bcc system it does not.

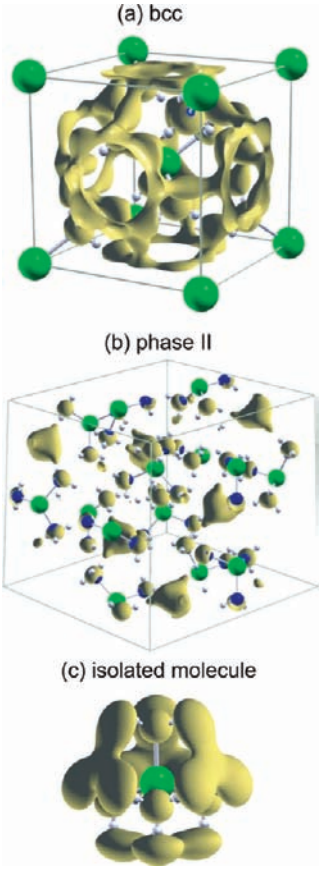

Figure 5. Isosurfaces of the valence occupied charge density for solid $Li(NH_3)_4$ in the (a) bcc (0.0069 e/Å^3) and (b) optimized phase II (0.0087 e/Å^3) structures as well as for the (c) isolated $Li(NH_3)_4$ molecule (0.003 e/Å^3).

on the $Li(NH_3)_4$ SOMOs happens to be near the center of the cavities, whereas for the other geometries this is not the case.

As Figure 5 shows, a substantial part of the electron density is in the interstitial regions (the rest is around the nitrogen atoms). Thus, solid $Li(NH_3)_4$ can be thought of as an electride. Electrides are a fascinating set of materials, in which distinct electrons play a structural and electronic role. There are organic[25−27] and inorganic[28] examples. The former include salts of alkali metals with ethers, cryptates, or their nitrogen analogues, and the latter nanoporous $[Ca_{24}Al_{28}O_{64}]^{4+}(4e^-)$. The high pressure forms of Li[29−31] and Na[32,33] may also be thought of as electrides, since in these cases the valence electrons are impelled into the interstitial regions due to the overlap of the core 1s and 2p orbitals, respectively. In Cs−IV, which has undergone a pressure induced electronic $s \rightarrow d$ transition,[34] the valence electrons are also found in the interstitial regions.[35]

5. SOLID $Li(NH_3)_4$ UNDER PRESSURE

Given the remarkably low−melting $Li(NH_3)_4$ solid, and notwithstanding the complexities of its structure, it is intriguing to explore the behavior of this expanded metal under compression. We examined the various geometries previously mentioned up to pressures of 200 GPa.

As Figure 6 shows, out of all of the structures we considered, phase II $Li(NH_3)_4$ was the most stable across the whole pressure range. Under compression, the x-parameter changed only very slightly, ranging from 0.125 to 0.133. In the following section we discuss the structural changes which occur under pressure and the ensuing electronics in greater detail.

We found the second most stable phase to be bcc−$Li(NH_3)_4$ (at 1 atm it has the same energy as the 'Cs−IV' structure). At normal pressures bcc is nearly isoenergetic to phase II; however, with increasing pressure the enthalpy difference between the two becomes progressively larger. In fcc−$Li(NH_3)_4$ four ammonias

dx.doi.org/10.1021/ja109397k |J. Am. Chem. Soc. 2011, 133, 3535–3547

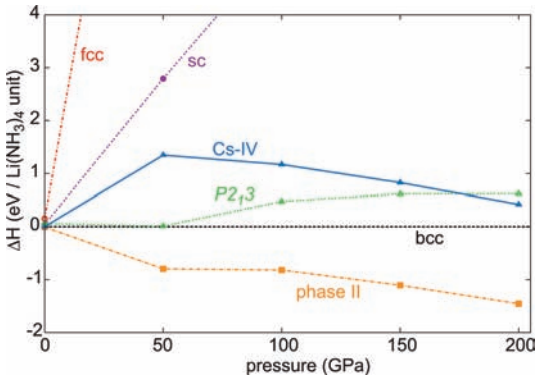

Figure 6. The enthalpies (in eV per $Li(NH_3)_4$ unit) of various solid $Li(NH_3)_4$ structures as a function of pressure. The enthalpies are given with respect to bcc−$Li(NH_3)_4$ at the specified pressure. The points represent calculated values, and the lines are given to guide the eye. The closeness of the enthalpies of many distinct structures at 1 atm is consistent with the fact that $Li(NH_3)_4$ has the lowest melting point of any known metal.

on different $Li(NH_3)_4$ units are oriented in such a way so that they face toward the center of a tetrahedron. The distances between two hydrogens (which point directly toward each other) in this configuration is 2.589 Å at 1 atm. Upon compression these hydrogens come prohibitively close to one another. At 200 GPa, the hydrogens "bend backwards" forming agostic bonds to Li, with an Li−N−H angle of 69°, and a nearest neighbor H−H distance of 1.13 Å. If they were to keep their normal Li−N−H angle of 113°, the hydrogen nuclei would surely overlap. Thus, the relative enthalpy of this structure is particularly high. At 200 GPa, the hydrogens in sc−$Li(NH_3)_4$ are quite close to each other with an H−H distance of 1.05 Å and an Li−N−H angle of 117°. In the Cs−IV/$P2_13$ structures, these values are 1.37/1.24 Å and 67/≥85° at the highest pressures considered. Cs−IV and $P2_13$ have lower enthalpies than the fcc and sc orientations.

A general point that should be kept in mind is that the favored geometries will in general be dependent upon Z (the number of molecular units in the unit cell). And, that no definitive conclusions can be reached on structural stability until the programs used for optimization can consider structures with a large Z. Consider for instance the bcc structure. The primitive cell has Z = 1, the conventional centered cell Z = 2. We showed earlier (Figure 2) how a deformation of the bcc structure can lead to the Z = 8 phase II. The bcc system whose enthalpy is shown in Figure 6 is highly constrained by setting Z = 1 in our calculations. We think that if Z were increased for bcc, and the system were allowed to deviate from bcc symmetry during the structural optimization, it would no doubt at some pressure merge with the phase II curve.

6. ELECTRONIC STRUCTURE AND METALLICITY OF $Li(NH_3)_4$ UNDER PRESSURE: AN UNEXPECTED SET OF BANDS

The behavior of the DOS of the most stable structure upon compression has some real surprises in it. Up to ∼100 GPa, the bandwidth of the valence states, and of the lowest set of unoccupied states of phase II $Li(NH_3)_4$ becomes narrower, as Figure 7 reveals. The bandwidth of the other occupied states, on the other hand, increases. Interestingly, at 50 and 100 GPa the phase II structure appears to be a semimetal, with a nearly negligible DOS at E_F. A blow−up of the DOS near the Fermi level (Figure 4 of the SI) reveals that it has a free electron−like parabolic onset up to 100 GPa, but at higher pressures the onset is sharp, almost one−dimensional. Moreover, at 150 and 200 GPa the bandwidth increases somewhat and the system becomes more metallic. Due to the extensive computational effort involved, we have not been able to use automated search techniques (genetic algorithms, random structure searches) in order to determine the most stable structural alternatives. We have also not been able to consider other (larger) unit cells. It is therefore not unlikely that at the highest pressures studied here a further structural distortion will lead to a semimetal with a lower enthalpy than phase II.

Now, here's the bigger surprise: under pressure a large gap opens up between the states just above the Fermi level and those higher in energy. This gap is already evident at 5 GPa. In phase II, there are eight formula units in the primitive cell. The occupied part of the valence DOS shown in Figure 4 of the SI integrates to eight electrons. The unoccupied part integrates to four electrons. Thus, there is a pronounced four−below−two band splitting, with a large gap separating these six bands from two more $4a_1$−based bands above.

Let us try to relate the decreased metallicity of compressed $Li(NH_3)_4$ with the structural changes that occur under pressure, focusing on the systems at 50 and 200 GPa. Their unit cells look basically the same as the one at 0 GPa in Figure 5(b), except that the lattice constants and distances between the atoms have decreased. In order to interpret the complex coordination environments that evolve at high pressures, we computed histograms of Li−N, N−H, Li−H, and H−H separations. These, shown in the SI to this paper, help us reach an appreciation of the structural changes caused by pressure. Table 2 lists the distances between selected atoms at 0, 50, and 200 GPa.

At 50 GPa the $Li(NH_3)_4$ molecules remain pretty much as they were at 1 atm, except that the Li−N distance decreases to 1.77/1.82 Å from their 1 atm value of 2.12 Å. The molecule appears to be mechanically "soft", with the Li−N (but not the N−H) distance responding to pressure.

At 200 GPa, more drastic changes are seen. The four Li−N bonds are now 1.58/1.62 Å, a half of an Ångstrom down from their P = 1 atm value. A fifth nitrogen gets close to each Li, such that the second nearest Li−N separation is 2.23 Å. And while the ammonia units remain pretty much intact, some H atoms come close to those of another Li (each Li has three hydrogens 1.63 Å away, and three more a bit further out at 1.83 Å). For comparison, we calculate the Li−H distance in solid ionic LiH to be 1.94 Å at normal pressures and 1.61 Å in the diatomic molecule. Even though the concept of a coordination number is not well−defined, it appears that the Li atoms are approaching eleven−fold coordination (five N and six H atoms). As the pressure is increased, van der Waals space between the $Li(NH_3)_4$ units is squeezed out, and the coordination of the lithiums increases, according to the hierarchy proposed in ref 36.

Computations predict that when pure ammonia is subject to pressures ranging from 90 to 450 GPa, layers of NH_4^+ and NH_2^- ions will form.[37] Up to 200 GPa, we do not see this occurring in $Li(NH_3)_4$, and every nitrogen atom remains bonded to three hydrogens when compressed.

In Figure 8 we show isosurfaces of the valence electron density of phase II at 50 and 200 GPa (i.e. in an energy window of $-2 \leq \varepsilon \leq 0$ eV). Whereas at 1 atm, all of the Li−N bonds are nearly equidistant (2.120 vs 2.121 Å), under pressure the difference between the two types of bonds increases to ∼0.05 Å. We find there to be substantially less electron density around the nitrogens with slightly longer Li−N bonds (the red ones in the figure) and the hydrogens bonded to them. With increasing pressure, the

dx.doi.org/10.1021/ja109397k | J. Am. Chem. Soc. 2011, 133, 3535–3547

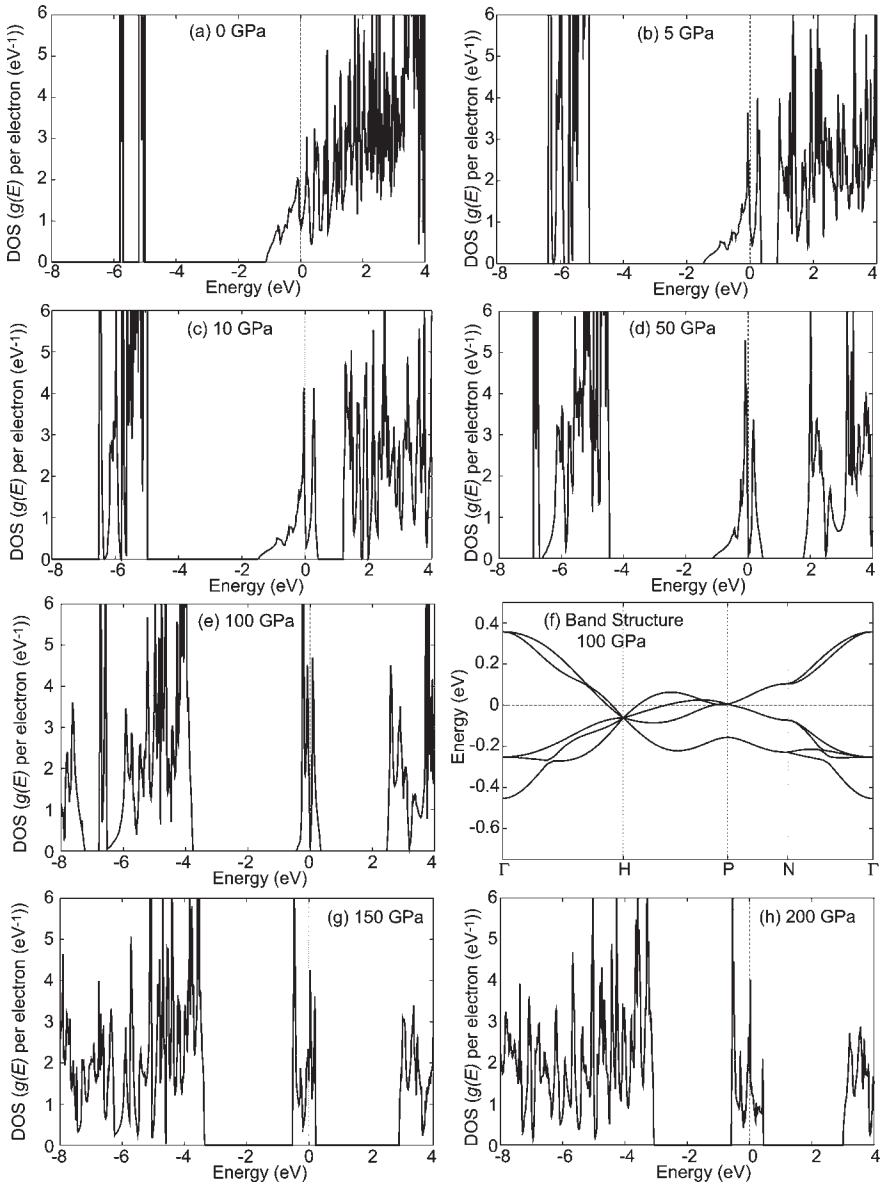

Figure 7. Valence DOS ($g(E)$/excess electron in eV^{-1}) of the optimized geometries of phase-II $Li(NH_3)_4$ at (a) 0, (b) 5, (c) 10, (d) 50, (e) 100, (g) 150, and (h) 200 GPa. The dashed vertical lines is the Fermi energy, E_F. At these pressures the lattice parameters are: 15.193, 12.563, 11.895, 10.282, 9.578, 9.170, and 8.890 Å, respectively. (f) The band structure of phase II at 100 GPa. Note the four−below−two band splitting around E_F, and the large gap between these six bands, and those above.

red nitrogen atoms approach a Li belonging to another $Li(NH_3)_4$ complex. Shortly we will discuss the blue nitrogen atoms and the hydrogens which are bonded to them.

7. HYDROGEN−LINED POCKETS IN $Li(NH_3)_4$ UNDER PRESSURE

We want to find the source of the mysterious six isolated bands in phase II $Li(NH_3)_4$ under pressure (Figure 7(e)). Interestingly, the valence DOS of the phase II structure, but with the Li atoms removed, and an overall charge of minus eight ($8[(NH_3)_4^-]$) is nearly the same as the valence DOS in Figure 7 (see the SI). This suggests that the answer to our question may lie in the ammonia molecules themselves. In fact, the valence DOS can be understood by taking into account only some of the ammonias—those colored in blue, as described below.

Even in Figure 8, as complicated and messy as it is, we can see that the hydrogens bonded to the nitrogens colored in blue are not equivalent. Most of the valence electron density resides on one of the hydrogens in a given NH_3 group. Four of these hydrogens from different NH_3 units come very close to each other (1.70−2.00 Å and 1.23−1.29 Å at 50 and 200 GPa, respectively). The distances between the hydrogens are quite similar to the closest intermolecular H−H distances in pure H_2 solid alone. We calculated 1.65 and 1.18 Å for the $P6_3/m$ (50 GPa) and $C2/c$ (200 GPa), which were determined to be the most stable structures for H_2 at these pressures.[21] For comparison the interatomic distance in an H_2 molecule was calculated to be 0.75 Å, the experimental value is 0.74 Å.

These hydrogens form a pocket or cavity, and there are precisely six such pockets of two distinct types in the unit cell. The location of

dx.doi.org/10.1021/ja109397k |J. Am. Chem. Soc. 2011, 133, 3535–3547

Table 2. Distances (Å) between Selected Atoms and Number of Such Contacts in the Phase II Structure at 0, 50, and 200 GPa

	0 GPa	50 GPa	200 GPa	number of contacts
Li−Li	5.37	3.46	3.15	3
	6.58	4.45	3.85	2
Li−H[a]	3.50	1.94	1.63	3
	2.69	2.28	1.83	3
Li−N	2.12	1.77	1.58	3
	2.12	1.82	1.62	1
	4.46	2.63	2.23	1
N−H[b]	1.03	1.02	0.98	3
N−H[b]	1.03	1.00	0.98	1
	1.03	1.01	1.01	1
	1.03	1.08	1.09	1

[a] At normal pressure the hydrogens within the $Li(NH_3)_4$ unit are closer to the Li than those in other units (Li−H ~2.7 Å). Under pressure the van der Waals space is squeezed out, and the hydrogen atoms from another monomer unit approach the Li atoms. For consistency we provide the distance between the same Li and H atoms at all pressures, even though at 0 GPa there may be other Li−H contacts which are shorter. [b] There are two distinct nitrogen atoms colored in blue and red in Figure 8.

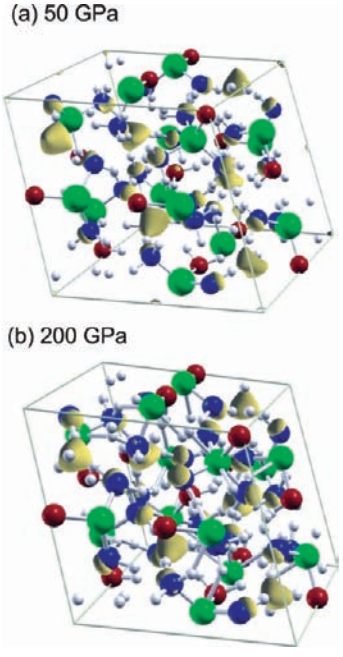

Figure 8. Isosurfaces of the valence occupied charge density for phase II of solid $Li(NH_3)_4$ at (a) 50 GPa, $v/v_0 = 0.31$ (0.09 e/Å^3), and (b) 200 GPa, $v/v_0 = 0.25$ (0.15 e/Å^3). Li atoms are colored green, and hydrogens white. There are two distinct nitrogens. At 50 GPa: Li−N_{blue} = 1.77 Å, and Li−N_{red} = 1.82 Å. At 200 GPa: Li−N_{blue} = 1.58 Å, Li−N_{red} = 1.62 Å.

these pockets is given in Figure 9 for $P = 100$ GPa. In order to ease visualization, the two interpenetrating nets of $Li(NH_3)_4$ molecules are given by the green and blue pseudoatoms (as in Figure 3) and the location of the pockets by the red balls.

In Figure 10(a) we show the atomic positions of the ammonias defining one of these pockets—the more symmetrical one located on a $\bar{4}$ axis. Note the D_{2d} distorted tetrahedron of close H⟵〰⟶H contact. We proceeded to model the pocket by

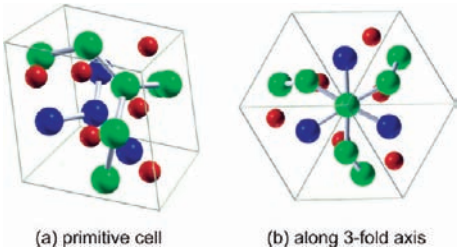

Figure 9. The blue and green pseudoatoms represent the center of the $Li(NH_3)_4$ monomers, which form two interpenetrating nets in the phase II structure. The red balls have been placed at the center of the six pockets. These are the areas where H⟵〰⟶H bonding interactions between nearby $Li(NH_3)_4$ units give rise to a substantial valence electron density. The lines are given to guide the eye and do not represent bonds.

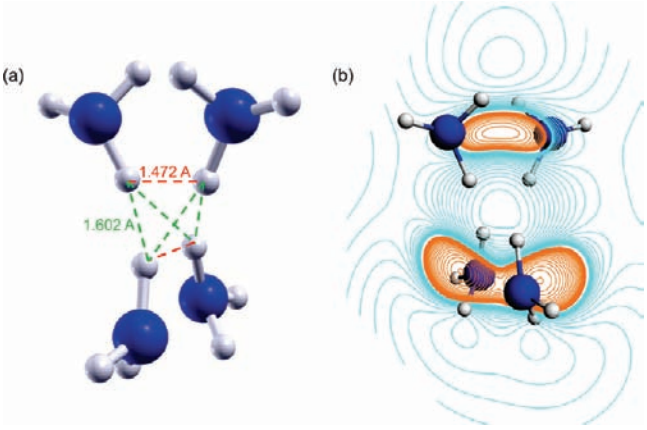

Figure 10. (a) The geometrical arrangement of the ammonia molecules surrounding one of the pockets containing a large amount of electron density in phase II $Li(NH_3)_4$ at 100 GPa. Four hydrogens point toward each other giving rise to a distorted tetrahedron with four H−H distances of 1.602 Å and two of 1.472 Å. (b) A contour diagram of the SOMO of $e^-@(NH_3)_4$ with the same geometry as in Figure 10(a). The contour passes through the middle of the pseudo−tetrahedron, where it displays a maximum.

performing a molecular calculation on $e^-@(NH_3)_4$, fixing the geometry to be the same as in phase II at 100 GPa.

The a_1 SOMOs of the monomers surrounding the pocket—here modeled by a single ammonia group each—combine to give a "super−a_1" orbital, whose contours are shown in Figure 10(b). In our model calculations this orbital is occupied by one electron. In contrast to our former findings on optimized square planar and tetrahedral $e^-@(NH_3)_4$ geometries,[1] the electron density in the constrained system displays a maximum in the center of the cavity. Whereas the nearest neighbor H−H distance in the optimized square planar configuration was 3.89 Å, here it is much closer: 1.60 Å. Perhaps this is one reason for the very different electron distributions between the optimized and the compressed model systems.

Above the a_1 orbital, and separated from it by some 0.4−0.55 eV, lie three orbitals that look just like the p_x, p_y, p_z orbitals of an isolated pseudoatom. Since our system does not have spherical symmetry, their energies are nondegenerate.

Interaction of the "super−a_1" atomic orbitals will give rise to six bands in the primitive unit cell of phase II-$Li(NH_3)_4$. These are filled with eight excess electrons from the lithium atoms, yielding the band structure illustrated in Figure 7. Below we will illustrate that it is possible to obtain a pretty good description of this unique

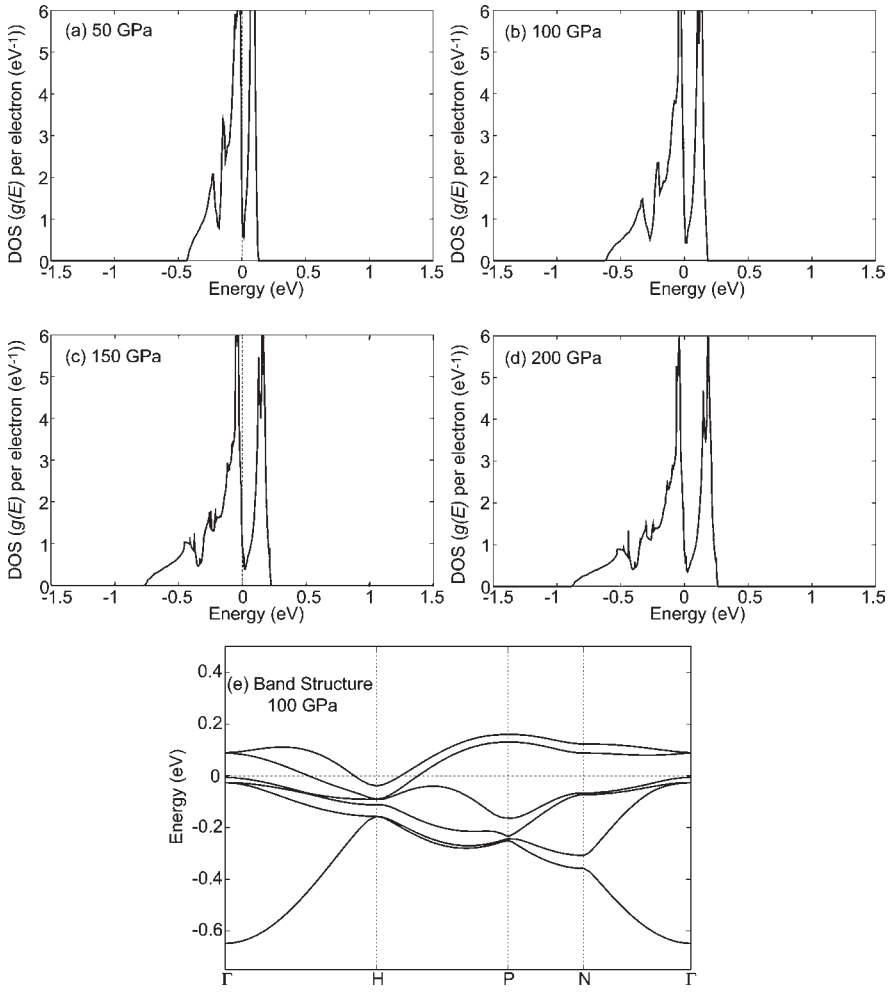

Figure 11. Valence DOS ($g(E)$/excess electron in eV^{-1}) of an $(H_6)^{2-}$ lattice. The hydrogen atoms have been placed in the cavities containing the maximum electron density arising from H⟵⟶H bonding interactions in phase-II $Li(NH_3)_4$ at (a) 50, (b) 100, (c) 150, and (d) 200 GPa. (e) The band structure corresponding to Figure 11(b). The dashed vertical lines is the Fermi energy, E_F.

band structure by maintaining even less molecular detail and focusing on only the pockets themselves.

8. THE POCKETS INTERACT: A SIMPLE MODEL

The effect of pressure on equilibria involving solvated electrons has been examined experimentally (see ref 38 and references therein). Stacy, Johnson, and Sienko have employed the Jortner model to predict that solid $Li(NH_3)_4$ should become less metallic when compressed.[11] Let us explain how they came to this conclusion. Jortner assumed that the excess electron is trapped within a spherical cavity of ammonia molecules which it polarizes.[39] This gives rise to a centrally symmetric potential which can be written as $V(r) = -e^2/K_{eff}R$ for $r < R$ and $V(r) = -e^2/K_{eff}r$ for $r \geq R$, where R is the cavity radius, and K_{eff} is a sum of the low and high−frequency dielectric constants. Stacy et al. reasoned that as the density of $Li(NH_3)_4$ becomes greater (either by lowering the temperature or by increasing the pressure), the cavity radius becomes smaller, and the potential well of the cavity deeper. Since it would be energetically more favorable for the electrons to reside in the cavities, the system would become less metallic.[11] The observation that lithium−methylamine solutions are less metallic than metal−ammonia ones has also been explained by the difference in the degree of confinement the excess electron experiences in these two solvents.[40] In a recent review, Edwards and co-workers have described ways to think about the metal to insulator transition.[41]

Can we also explain the peculiar electronic structure of phase II under pressure—the decreased metallicity and the marked segregation of states (four−below−two splitting) evident in the DOS illustrated in Figure 7—using a Jortner−like model? In order to do so we again consider the pockets of maximum electron density which arise due to intermolecular H⟵⟶H bonding interactions between nearby $Li(NH_3)_4$ units described in the preceding section. At each pressure considered, the phase II systems each consist of exactly six of these pockets and eight $Li(NH_3)_4$ molecules per primitive unit cell. The location of these pockets or holes has already been pointed out — they are the red balls in Figure 9.

We now assume that the eight excess electrons reside completely within the six voids. Computationally, this can be approximated by $(H_6^*)^{2-}$: a structure where hydrogen atoms — call them pseudoatoms, H*, — have been placed in the middle of the pockets and which contains eight valence (excess) electrons. The resulting $R3$ structure (space group 146) has two distinct hydrogen H* centers at (0.959, 0.792, 0.417) and (0.284, 0.841, 0.568).

We have calculated the DOS for such model systems at the different pressures considered within this work. At 0 GPa, the pseudoatoms are too far apart (the shortest separation between

dx.doi.org/10.1021/ja109397k |J. Am. Chem. Soc. 2011, 133, 3535–3547

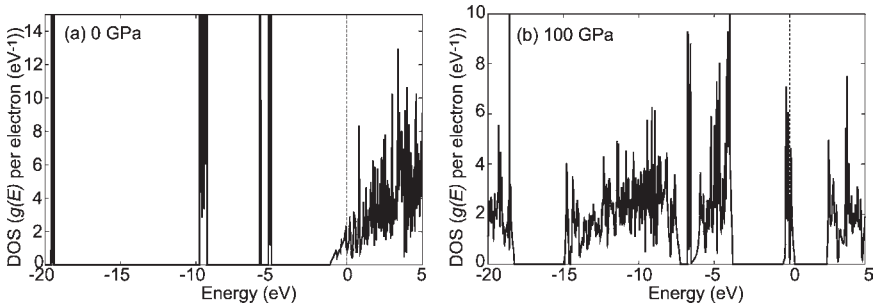

Figure 12. DOS ($g(E)$/excess electron in eV^{-1}) of the optimized geometries of phase-II $Li(NH_3)_4$ at (a) 0 and (b) 100 GPa. The dashed vertical lines is the Fermi energy, E_F. Note that the scale on the $y-$axis in the two subfigures is different.

them is 6.81 Å) to interact. The DOS of the 50−200 GPa "hydrogen−in−the−holes" geometries given in Figure 11 is remarkably similar to that for the phase II systems in Figure 7 (see also Figure 4 of the SI). The region shown corresponds to the six bands formed from the interaction of the hydrogen $s-$orbitals. Four of these bands are occupied and the Fermi level falls in a pseudogap. There is a large gap between these six levels and those derived from the $p-$orbitals of the hydrogens used to model the cavities. Thus, the four−below−two splitting in the bands around E_F in phase II arises from the topology of the six cavities and their filling with eight excess electrons.

There are some differences between the model and the real system though. For example in going from 50 to 100 GPa in phase II, the valence DOS narrows because with increasing pressure the radius of the pockets decreases. On the other hand, for $(H_6^*)^{2-}$ the smaller lattice constant increases the interaction between nearby hydrogen atoms and the bands broaden. Above 150 GPa the bands in phase II broaden as well; however, this is probably due to structural changes in the $Li(NH_3)_4$ units at the highest pressures considered. The model system does not capture the one−dimensional onset of the DOS which occurs in the real system at 150 and 200 GPa. Comparison of the band structures also reveals differences between the real and model systems (see Figure 7(f) and Figure 11(e)).

We have now provided two ways which can be used to understand the peculiar electronic structure of the squeezed $Li(NH_3)_4$ — by considering the interaction of (i) "super−a_1" AOs made up of the ammonia LUMOs, or by (ii) a Jortner−like model where pseudoatoms reside in the cavities. Interestingly, our results suggest that perhaps adding 1/2 an electron more per Li to the compressed phase II structure could lead to a very stable insulating system. This could be accomplished by either partial substitution of Li (by, say, Be), or N (by O).

There is actually a third way which can be used to understand the pressure−induced narrow band formation in the initially free−electron part of the DOS of $Li(NH_3)_4$. Interestingly, both the DOS of compressed Li[24] and of phase II $Li(NH_3)_4$ at normal pressure display two pseudogaps: one at E_F and one at an energy which is slightly higher (E_F+2 and E_F+0.4 eV, respectfully). Feng et al. illustrated that it is possible to create narrow bands by deepening and widening the gaps via a pressure−activated Jones zone plane scenario.[42] With increasing pressure, the perturbation caused by the set of zone planes (the actual zone planes that cause the phenomenon remain to be identified) becomes so activated that actual gaps may form, and a band will narrow and split off, as is the case in phase II $Li(NH_3)_4$. The narrow bands are indicative of localization of the initially free−electron like manifolds, as a result of the growth of the pseudogap as the system is compressed.[42]

9. THE "CORE" MOS OF $Li(NH_3)_4$ UNDER PRESSURE

In elemental Li, the 1s cores start to overlap with increasing pressure, and the valence electrons are pushed into the interstitial regions.[29−31] Thus, compressed Li can be thought of as an electride. Upon compression the 1s bandwidth increases, whereas the 2s is actually found to decrease. Recent experiments have shown that Li even becomes semiconducting at around 80 GPa.[43]

The situation is similar to what we observe here; however, the Li atoms in $Li(NH_3)_4$ are too far apart for the Li 1s cores to overlap. But what about the $Li(NH_3)_4$ 'core MOs'? Compare the DOS of the phase II structure at 0 and 100 GPa viewed in a wider energy window than Figure 7, in Figure 12. The features near −5 eV are due to the $3a_1$ and $3t_2$ orbitals of the monomer (made up mainly of the NH_3 lone pairs and the Li 2s/2p) which are close to each other — but not identical — in energy. The peaks around −10 eV are from the $1t_1$, $1e$, and $2t_2$ MOs of $Li(NH_3)_4$, a total of 8 orbitals per monomer unit. At normal pressures, the peaks in the DOS below −5 eV are nearly delta functions. Under pressure, these states become quite broad, indicating that overlap between the 'core MOs' in $Li(NH_3)_4$ does indeed occur. The pressure on the "outside" is communicated to the interior of the molecule.

10. LOW DIMENSIONAL STRUCTURES: 1D CHAINS AND 2D SHEETS OF $Li(NH_3)_4$

While discussing the excited states of both the solvated electron, and $Li(NH_3)_4$ in a previous paper, we fell naturally into the language of superatoms.[1] The tetrahedral $Li(NH_3)_4$ units are quasi−spherical. The $4a_1$ SOMO is like a (big) $s-$orbital, and the triply degenerate $4t_2$ LUMOs are like (big) $p-$orbitals centered on the entire $Li(NH_3)_4$ unit. As we saw in previous work, these MOs extend outside the component atoms.[1] They can therefore be thought of as superatom molecular orbitals or SAMOs. Such orbitals are MOs of the system that look like "united−atom" or centered MOs but extend pretty far outside the atom positions in the molecule.

Recently, experimental evidence for the existence of SAMOs in C_{60} molecules has been provided.[44] Whereas in the fullerenes the SAMOs lie at least 3 eV above the C_{60} LUMO, in $Li(NH_3)_4$ molecules, they are the frontier orbitals. Subsequently, theoretical calculations performed on chains and sheets composed of these C_{60} units studied how the SAMOs interact to form nearly

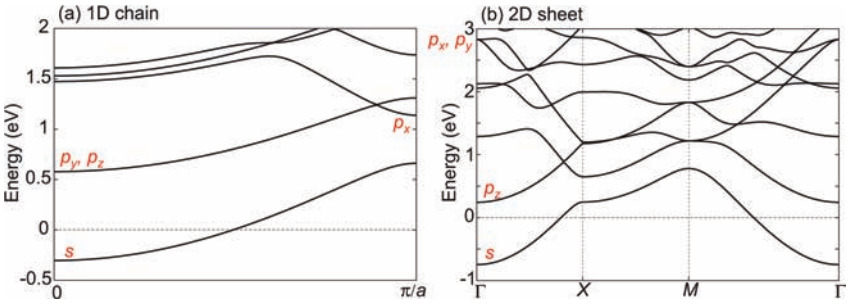

Figure 13. The band structure of a (a) 1D chain and (b) 2D sheet made up of $Li(NH_3)_4$ units. The energy bands formed by the s, p_x, p_y, p_z SAMOs are pointed out.

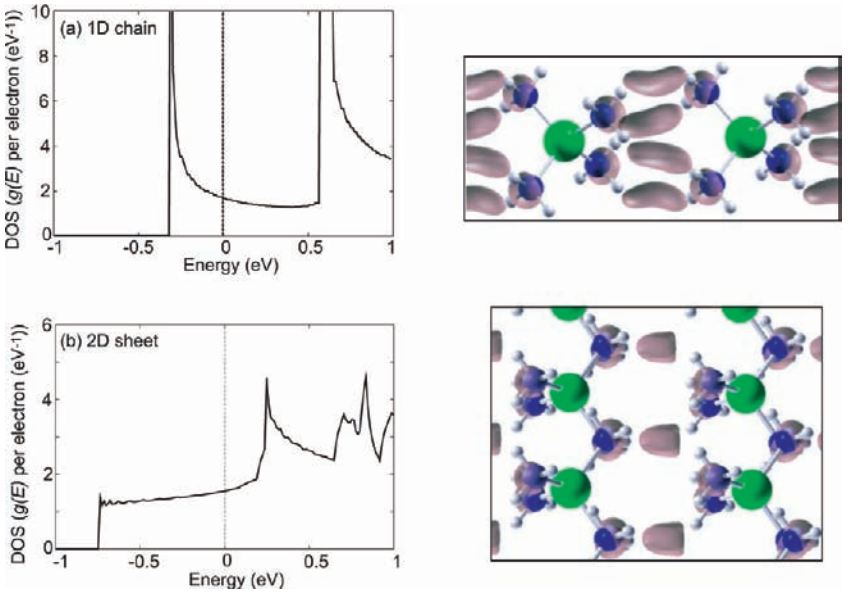

Figure 14. Valence DOS ($g(E)$/excess electron in eV^{-1}) and isosurfaces of the valence occupied charge density for a (a) 1D chain (0.007 $e/Å^3$) and (b) 2D sheet (0.014 $e/Å^3$) made up of $Li(NH_3)_4$ units.

free electron bands.[45] Other superatom systems such as $Al_{13}I_x^-$, $Al_{14}I_3^-$[46] and $AlPb_{10}^+$, $AlPb_{12}^+$[47] have also been previously studied. For a review of the superatom literature see ref 48.

We wanted to study low−dimensional structures of $Li(NH_3)_4$ in order to determine how far we could push the connection to SAMOs. This would also allow us see the development of metallicity in the extended systems as the dimensionality is varied. The formation energy of a 1D chain, and a 2D sheet, from isolated $Li(NH_3)_4$ molecules was calculated as being −0.285 and −0.466 eV per $Li(NH_3)_4$ unit, respectively. The magnitude of the formation energies is lower than any of the optimized three-dimensional solids considered in Table 1, as expected.[23] This suggests that the $Li(NH_3)_4$ units prefer still higher coordination numbers than those made available by our restriction of these systems to one−and two−dimensional lattices. This occurs since the three−dimensional systems allow for more H⟵⟶H -bonding interactions. Both of the low dimensional systems were found to be metallic, and Peierls distortions (likely to occur) were not considered for the 1D chain. The band structures along selected high symmetry lines in the Brillouin Zone (BZ) are plotted in Figure 13 for the wire and the sheet. Along lines connecting other high symmetry points, the bands show little dispersion since the $Li(NH_3)_4$ units are too far apart to interact.

Let us first consider the linear array, a quantum wire. Going from $k = 0−\pi/a$, the band made up from the interaction between the s-like $4a_1$ $Li(NH_3)_4$ SOMOs "runs up"[49] from the zone center, and it is half full. The doubly degenerate p_y/p_z band also runs up, as expected. The p_x (where x is the direction along the chain) band is predicted to "run down" from the zone center as a consequence of the topology of its orbital interactions. This is the band that falls below p_y/p_z at the zone edge. There are actually signs of a level crossing with the s band near the zone boundary. The frontier orbitals of $Li(NH_3)_4$ interact to form nearly free electron (NFE) like bands, as do the SAMOs of C_{60}.[45]

The Van Hove singularities in the DOS for the chain (Figure 14(a)) are a hallmark of 1D behavior. We have also plotted the electron density in the energy window $−0.35 \le \varepsilon \le 0$ eV in the right panel of Figure 14(a). It is clearly derived from an overlap of the $4a_1$ $Li(NH_3)_4$ SOMOs with a lobe around the nitrogen atoms, and intermolecular H⟵⟶H bonding interactions along the chain are evident.

Let us consider the 2D sheet. In Figure 13(b) we show the band structure along Γ−X−M−Γ. The s band runs up from Γ−X−M and then back down again. The p_z also runs up from Γ−X, then it is effectively flat to M, at which point it runs down again. At Γ the doubly degenerate band at almost 3 eV above E_F is most

dx.doi.org/10.1021/ja109397k |J. Am. Chem. Soc. 2011, 133, 3535–3547

likely due to p_x and p_y. The former should run up, and the latter run down when going to X; however, hybridization with other d−like bands splits up the bands a bit. The step−like DOS in Figure 14(b) is characteristic of 2D structures. Once again, the electron density arising from the bands formed from the SOMO that are filled exhibits H←〰→H bonding interactions between nearby hydrogen atoms. The right panel shows that pockets of electron density arise in regions which are surrounded in a tetrahedral fashion by NH_3 units.

In both of these low−dimensional structures, the diffuse s and p−like SOMOs and LUMOs interact to form NFE−like bands. Isosurfaces of the occupied valence electron density show H←〰→H bonding interactions, as we saw previously in molecular clusters, and now here in the 3D systems.

11. WHAT KIND OF METAL IS THIS?

From the point of view of metal physics, the building block of this metal, $Li(NH_3)_4$, is a most unusual beast. It is a roughly spherical chunk of matter of radius around 4 Å (max of $P(r)$), which carries a single electron in a quasispherical s−type orbital that reaches out more than 6 Å from the center (see Figure 13 in ref 1). And it has low−lying empty p−type orbitals. As one would expect, $Li(NH_3)_4$ has a high polarizability, calculated by us to be 146.1 Å^3. The same computational settings yield polarizabilities of 20.0 Å^3 and 51.3 Å^3 for Li and Cs. The large polarizability of $Li(NH_3)_4$ implies both ready metallization by the Goldhammer−Herzfeld criterion and the presence of large dispersion forces between monomers. We have also calculated the polarizabilities of the $Li(NH_3)_4$ monomers obtained from the optimized phase II structures at 100 and 200 GPa. Under pressure the Li−N bond lengths decrease, as does the radius of the monomer. It is therefore not surprising that the polarizability also decreases to 74 Å^3 and 54 Å^3 at the aforementioned pressures.

$Li(NH_3)_4$ is a most unusual metal, as its low melting point indicates. In a separate contribution Peter Edwards and the authors will take a careful look at the experimental measurements of conductivity and transport properties in solid $Li(NH_3)_4$. We will reconcile the high polarizability of the monomer with its low melting point and take a look at how the phonons influence the melting. A detailed comparison to the alkali metals themselves and to other metallic molecular systems will help to delineate the strangeness of $Li(NH_3)_4$.

It has not been easy to study the electronic structure of solid $Li(NH_3)_4$ at normal conditions, and under pressure, for the system opts for structural complexity. And, consistent with this material being the lowest melting liquid metal known, many ordered structures are of nearly equal energy, at least at $P = 1$ atm.

Experiments have shown that phase II (25−82 K) crystallizes in the space group $I\bar{4}3d$. Out of all of the systems which we studied, this $Z = 8$ structure was found to have the lowest energy (a geometry optimization of the structure proposed for phase III with $Z = 16$ were too expensive to perform). Our work confirms the results of recent experiments which show the molecular building block in phase II to deviate only slightly from tetrahedral symmetry.[9] The phase II structure is as beautiful as it is complex and can be thought of as two tightly−coupled interpenetrating trigonal nets of $Li(NH_3)_4$ monomers. Close in energy to this structure emerge bcc and "Cs−IV" alternatives. The material is metallic, but the Fermi level is in a pseudogap, confirming Sienko's characterization of it as a poor metal.[11]

Under pressure, the $I\bar{4}3d$ structure becomes more stable than its competitors. And, remarkably, a set of six relatively flat bands (for $Z = 8$) separate themselves from the others, with significant gaps above and below. The Fermi level corresponds to occupation of four out of six of these bands. We trace the bands to precisely six pockets in the $Z = 8$ structure. These are derived from four different NH_3's which are forced close to each other, forming rough tetrahedral pockets lined by one hydrogen from each ammonia. Each of the six pockets has a characteristic pseudo−s−type orbital, with electron density maximal in the center of the pocket; the six bands arise from these six pseudo−s orbitals. And they are filled with eight electrons. Adding 1/2 electron more per Li atom to the compressed phase II could lead to a very stable system.

We show that low−dimensional systems made up of $Li(NH_3)_4$ units give rise to band structures which have the same characteristics as those derived for wires or sheets of hydrogen atoms. That is, the frontier orbitals of $Li(NH_3)_4$ can be thought of as superatom molecular orbitals.

We look forward to experimental investigations of $Li(NH_3)_4$ under pressure. We have a feeling that there are more surprises lurking in the metallicity of the solid phases of this low−melting metal.

12. COMPUTATIONAL DETAILS

Geometry optimizations and electronic structure calculations were performed using density functional theory (DFT), with the PBE exchange−correlation functional[50] as implemented in the VASP code.[51,52] The effects of electron correlation are approximated by our choice of functional. In a very wide−band system the consequences of correlations can be minor compared with the band (or kinetic energy) terms. The computations carried out herein cannot provide any insight into the electron correlation effects, nor about how they change with increasing/decreasing pressure. Plane−wave basis sets within the PAW method[53,54] were employed, with an energy cut−off of 750 eV. The $1s^1$, $1s^22s^1$, and $2s^22p^3$ electrons were all treated as valence for H, Li, and N, respectively. The k−point grids were generated using the Monkhorst-Pack scheme, and the number of divisions along each reciprocal lattice vector was chosen so that the product of this number with the corresponding real lattice constant was about 50 Å. For calculations on the isolated $Li(NH_3)_4$ a simple cubic cell with a lattice parameter of 20 Å was employed. We have also considered 1D sheets and 2D solids. For the former, the distance in−between Li atoms in the chain was allowed to vary in the x-direction, and the total volume of the cell was fixed to be 2400 Å^3 in the optimization. This led to a rectangular cell with $a = 6.02$ Å, $b = c = 19.96$ Å. For the latter, the x and y-directions were allowed to optimize, and the volume of the rectangular cell was fixed to 720 Å^3. The optimized cell parameters were $a = b = 6.13$ Å, $c = 19.14$ Å.

For most of the data presented herein, we are using plane−wave calculations in order to study the extended structures. Thus, we first redid the discrete molecules which we studied in ref 1 with the same plane−wave scheme. The optimized structural parameters obtained in the periodic calculations (Li−N: 2.10 Å, N−H: 1.03 Å, H−N−Li: 112.9°, and H−N−H: 105.9°) agree well with those from the molecular ones calculated with the revPBE functional (Li−N: 2.11 Å, N−H: 1.03 Å, H−N−Li: 113.3°, H−N−H: 105.4°). For the discrete molecules, other GGA functionals (BLYP, BP86, PBE, PW91, RPBE) also yielded a Li−N bond length of 2.11 Å, whereas the one we computed with LDA was somewhat shorter (2.02 Å). This is not surprising since the LDA is known to overbind. For comparison, the Li−N bonds found with B3LYP and MP2 in ref 16 were 2.09 and 2.07 Å, respectively.

The static polarizability for $Li(NH_3)_4$ was obtained from a complete TDDFT sum−over−states (SOS),[55] which is equivalent to calculating the polarizability directly from linear response.[56] The SOS approach was taken

because analytic polarizabilities of open shell systems can presently not be performed with the ADF code. This molecular calculation was carried out using the same computational settings (functional, basis set) as in ref 1.

■ ASSOCIATED CONTENT

Supporting Information. Discussion of the results obtained for the strongly distorted $Li(NH_3)_4$ complex; densities of states for various phase II structures at 0 GPa; histograms of the Li−N, N−H, Li−H, and H−H distances in the phase II structure at various pressures; densities of states of the phase II structures under pressure; structural parameters and enthalpies of all of the $Li(NH_3)_4$ systems which we considered. This material is available free of charge via the Internet at http://pubs.acs.org.

■ AUTHOR INFORMATION

Corresponding Author
ezurek@buffalo.edu

■ ACKNOWLEDGMENT

We are grateful to Peter Edwards, Matthew Lodge, Neil Ashcroft, and William I. F. David for insightful discussions. We thank Ji Feng for carrying out the first computations on $Li(NH_3)_4$. Ji Feng also provided insightful comments on the manuscript and brought up the idea that the narrow bands in the phase II structure are a result of Brillouin Zone plane activation. For funding the research we thank the National Science Foundation Grants CHE-0910623 and DMR-1005413. This research was also supported in part by the NSF through TeraGrid resources provided by NCSA. E.Z. acknowledges support from the Center of Computational Research (CCR) at SUNY Buffalo.

■ REFERENCES

(1) Zurek, E.; Edwards, P. P.; Hoffmann, R. *Angew. Chem., Int. Ed.* **2009**, *48*, 8198–8232.
(2) Joannis, M. A. *C. R. Acad. Sci.* **1889**, *109*, 900–902.
(3) Moissan, H. *C. R. Acad. Sci.* **1898**, *127*, 685–693.
(4) Mammano, N.; Sienko, M. J. *J. Am. Chem. Soc.* **1968**, *90*, 6322–6324.
(5) Glaunsinger, W. S.; Von Dreele, R. B.; Marzke, R. F.; Hanson, R. C.; Chieux, P.; Damay, P.; Catterall, R. *J. Phys. Chem.* **1984**, *88*, 3860–3877.
(6) Stacy, A. M.; Sienko, M. J. *Inorg. Chem.* **1982**, *21*, 2294–2297.
(7) Chieux, P.; Sienko, M. J.; DeBaecker, F. *J. Phys. Chem.* **1975**, *79*, 2996–3000.
(8) Young, V. G.; Glaunsinger, W. S.; Von Dreele, R. B. *J. Am. Chem. Soc.* **1989**, *111*, 9260–9261.
(9) Ibberson, R. M.; Fowkes, A. J.; Rosseinsky, M. J.; David, W. I. F.; Edwards, P. P. *Angew. Chem., Int. Ed.* **2009**, *48*, 1435–1438.
(10) White, T. R.; Hsu, S. P.; Mobley, M. J.; Glaunsinger, W. S. *J. Phys. Chem.* **1984**, *88*, 3890–3895.
(11) Stacy, A. M.; Johnson, D. C.; Sienko, M. J. *J. Chem. Phys.* **1982**, *76*, 4248–4254.
(12) Stacy, A. M.; Edwards, P. P.; Sienko, M. J. *J. Solid State Chem.* **1982**, *45*, 63–70.
(13) Lemaster, E. W.; Thompson, J. C. *J. Solid State Chem.* **1972**, *4*, 163–171.
(14) Martyna, G. J.; Klein, M. L. *J. Phys. Chem.* **1991**, *95*, 515–518.
(15) Kaplan, T. A.; Harrison, J. F.; Dye, J. L.; Rencsok, R. *Phys. Rev. Lett.* **1995**, *75*, 978.
(16) Mierzwicki, K.; Latajka, Z. *Chem. Phys.* **2001**, *265*, 301–311.
(17) Kohanoff, J.; Buda, F.; Parrinello, M.; Klein, M. L. *Phys. Rev. Lett.* **1994**, *73*, 3133–3136.
(18) Takemura, K.; Minomura, S.; Shimomura, O. *Phys. Rev. Lett.* **1982**, *49*, 1772–1775.
(19) Olijnyk, H.; Holzapfel, W. B. *Phys. Lett. A* **1983**, *99*, 381–383.
(20) Ma, Y.; Oganov, A. R.; Xie, Y. *Phys. Rev. B* **2008**, *78* (014102), 1–5.
(21) Pickard, C. J.; Needs, R. J. *Nature Phys.* **2007**, *3*, 473–476.
(22) Chang, T. L.; Tung, L. H. *Nature* **1949**, *163*, 737.
(23) Wen, X. D.; Cahill, T. J.; Hoffmann, R. *Chem.—Eur. J.* **2010**, *16*, 6555–6566.
(24) Hanfland, M.; Syassen, K.; Christensen, N. E.; Novikov, D. L. *Nature* **2000**, *408*, 174–178.
(25) Dye, J. L. *Science* **2003**, *301*, 607–608.
(26) Dye, J. L. *Inorg. Chem.* **1997**, *36*, 3816–3826.
(27) Dye, J. L. *Acc. Chem. Res.* **2009**, *42*, 1564–1572.
(28) Matsuishi, S.; Toda, Y.; Miyakawa, M.; Hayashi, K.; Kamiya, T.; Hirano, M.; Tanaka, I.; Hosono, H. *Science* **2003**, *301*, 626–629.
(29) Neaton, J. B.; Ashcroft, N. W. *Nature* **1999**, *400*, 141–144.
(30) Pickard, C. J.; Needs, R. J. *Phys. Rev. Lett.* **2009**, *102*, 146401.
(31) Yao, Y.; Tse, J. S.; Klug, D. D. *Phys. Rev. Lett.* **2009**, *102*, 115503.
(32) Neaton, J. B.; Ashcroft, N. W. *Phys. Rev. Lett.* **2001**, *86*, 2830–2833.
(33) Ma, Y. M.; Eremets, M.; Oganov, A. R.; Xie, Y.; Trojan, I.; Medvedev, S.; Lyakhov, A. O.; Valle, M.; Prakapenka, V. *Nature* **2009**, *458*, 182–185.
(34) Sternheimer, R. *Phys. Rev.* **1950**, *78*, 235–243.
(35) Zurek, E.; Jepsen, O.; Andersen, O. K. *ChemPhysChem* **2005**, *6*, 1934–1942.
(36) Grochala, W.; Hoffmann, R.; Feng, J.; Ashcroft, N. W. *Angew. Chem., Int. Ed.* **2007**, *46*, 3620–3642.
(37) Pickard, C. J.; Needs, R. J. *Nat. Mater.* **2008**, *7*, 775–779.
(38) Böddeker, K. W.; Lang, G.; Schindewolf, U. In *Metal-Ammonia Solutions, Colloque Weyl II*; Ithaca, NY, 1969; Lagowski, J. J., Sienko, M. J., Eds.; Butterworths: London, 1970; pp 219−227.
(39) Jortner, J. *J. Chem. Phys.* **1959**, *30*, 839–846.
(40) Edwards, P. P.; Sienko, M. J. *J. Am. Chem. Soc.* **1981**, *103*, 2967–2971.
(41) Edwards, P. P.; Lodge, M. T. J.; Hensel, F.; Redmer, R. *Philos. Trans. R. Soc., A* **2010**, *368*, 941–965.
(42) Feng, J.; Hoffmann, R.; Ashcroft, N. W. *J. Chem. Phys.* **2010**, *132* (114106), 1–12.
(43) Matsuoka, T.; Shimizu, K. *Nature* **2009**, *458*, 186–189.
(44) Feng, M.; Zhao, J.; Petek, H. *Science* **2008**, *320*, 359–362.
(45) Zhao, J.; Feng, M.; Yang, J.; Petek, H. *ACSNano* **2009**, *3*, 853–864.
(46) Bergeron, D. E.; Roach, P. J.; Castleman, A. W.; Jones, N. O.; Khanna, S. N. *Science* **2005**, *307*, 231–235.
(47) Neukermans, S.; Janssens, E.; Chen, Z. F.; Silverans, R. E.; Schleyer, P. v. R.; Lievens, P. *Phys. Rev. Lett.* **2004**, *92* (163401), 1–4.
(48) Castleman, A. W.; Khanna, S. N. *J. Phys. Chem. C* **2009**, *113*, 2664–2675.
(49) Hoffmann, R. *Solids and Surfaces: A Chemist's View of Bonding in Extended Structures*; Wiley-VCH: New York, 1988.
(50) Perdew, J. P.; Burke, K.; Ernzerhof, M. *Phys. Rev. Lett.* **1996**, *77*, 3865–3868.
(51) Kresse, G.; Hafner, J. *Phys. Rev. B* **1993**, *47*, 558–561.
(52) Kresse, G.; Furthmuller, J. *Phys. Rev. B* **1996**, *54*, 11169–11186.
(53) Blöchl, P. *Phys. Rev. B* **1994**, *50*, 17953.
(54) Kresse, G.; Joubert, D. *Phys. Rev. B* **1999**, *59*, 1758–1775.
(55) Banerjee, A.; Autschbach, J.; Chakrabarti, A. *Phys. Rev. A* **2008**, *78*, 032704–9.
(56) Autschbach, J.; Seth, M.; Ziegler, T. *J. Chem. Phys.* **2007**, *126*, 174103–5.